Journal of Engineering Physics and Thermophysics, Vol. 79, No. 4, 2006

EXPERIMENTAL STUDY OF FLOW STRUCTURE AND HEAT TRANSFER UNDER A JET FLOW PAST A SPHERICAL-CAVITY OBSTACLE

V. I. Terekhov, V. L. Barsanov, S. V. Kalinina, and Yu. M. Mshvidobadze

UDC 536.24

The results of an experimental study of the aerodynamic characteristics and heat transfer under a jet flow past a spherical-cavity obstacle are presented. It has been revealed that in a spherical cavity the flow becomes nonstationary and is characterized by low-frequency oscillations of local values of the heat flow density. The heat transfer intensity in a hollow is lower than on a flat obstacle, and in the region of depression this decrease is practically completely compensated by an increase in the heat-transfer surface area.

One of the most effective ways of convective cooling of heat-stressed surfaces is the use of impinging jets. Up to now most study has been given to flow and heat transfer upon interaction of jets with a flat obstacle. In real articles, however, the jet-cooled wall can be far from flat. In the present work, the heat transfer between an axially symmetric jet and a spherical cavity is studied. Hollows have attracted the attention of the authors due to the fact that under a longitudinal flow they proved to be generators of unusual self-oscillation conditions and structures and effective heat-transfer intensifiers [1–3].

In the last few years, many researchers have given consideration to the formation, stability, and role of large-scale vortices (coherent structures) in the processes of heat and mass transfer in impinging jets [4, 5]. The presence of organized structures in a jet provides an additional possibility of controlling the heat transfer from the flown obstacle. As the analysis of the available publications, in particular [6], shows, such a control is possible by means of (time) periodic pressure perturbations imposed from the outside that influence the coherent structures in the jet, as well as by means of perturbations generated by the hydrodynamic interaction of the jet with an obstacle of complex shape.

Experimental studies of the interaction of impinging jets with curvilinear obstacles are represented by publications [7–11]. The authors of [7] took measurements of the pressure distribution and average heat transfer under air stream impingement and about a concave hemisphere which could be oriented at different angles to the stream. The Reynolds number constructed on the hemisphere diameter D_c was varied over the range of $\mathrm{Re}_D = 6\cdot10^3$–$9\cdot10^4$. The minimum heat transfer took place at a coaxial position of the jet and the hemisphere. Rotation of the hemisphere by 90^o could cause a threefold increase in the heat transfer. At an angle of 60^o a strong instability of the stream was observed and the experimental points dropped out of the general dependence of average heat transfer on the angle rotation.

In [8], the average and local heat transfer from the base of a cylindrical cavity oriented perpendicular to an unbounded free stream was determined experimentally. As the cavity depth Δ/D_c increased from 0 to 0.65, the heat transfer intensity decreased by a factor of more than 2, which the authors explained as the penetration of the stream inside the cavity and, accordingly, by the worsening of the heat-transfer processes between the base surface and the stream. The local distributions of the heat transfer coefficient along the cavity radius are highly nonuniform — their maximum is reached on the axis and their minimum at the periphery of the cavity base.

A detailed study of the flow structure, the recovery factor, and the heat transfer coefficient has been made in a series of investigations [9, 10], in which an axially symmetric jet interacted with cylindrical convex and concave surfaces. The temperature recovery coefficient was varied over a wide range — from 0.75 to 1.2 depending on the distance to a given surface, as well as on its shape. The authors have shown that the average heat transfer from the convex surface is higher by 20–50% than from the concave one, all other things being identical.

S. S. Kutateladze Institute of Thermal Physics, Siberian Branch of the Russian Academy of Sciences, 1 acad. Lavrentiev Ave., Novosibirsk, 630090, Russia; email: terekhov@itp.nsc.ru. Translated from Inzhenerno-Fizicheskii Zhurnal, Vol. 79, No. 4, pp. 29–37, July–August, 2006. Original article submitted May 3, 2005.

1062-0125/06/7904-0657

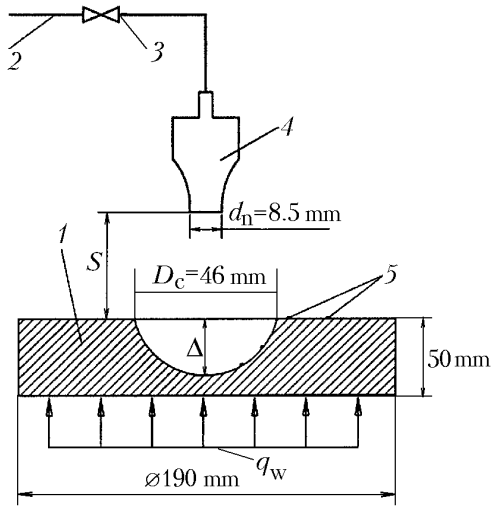

Fig. 1. Diagram of the experimental facility: 1) obstacle; 2) air line; 3) regulating valve; 4) nozzle; 5) heat flow sensors.

The experimental study performed in [11] is the closest to the present work. A hemispherical depression was blown by an air jet in the direction of the vertical axis of the cavity. The jet diameter at the outlet from the nozzle was much smaller than the depression diameter D_c/d_n = 16–50. According to the data obtained, the heat transfer at the stagnation point of the jet at a fixed Reynolds number depends on the distance between the nozzle and the obstacle. Compared to the flow past a flat surface the heat transfer in a spherical cavity decreases and the Reynolds number exponent in the relation for the heat exchange increases from n = 0.5 for a flat obstacle to n = 0.66 for a hemisphere at large diameters of the nozzle.

From the description of the results of the works it can be seen that the available publications contain mainly information on the average flow and heat exchange characteristics and do not give a clear idea of the complex gasdynamic and thermal processes of interaction of impinging jets with spherical depressions. It should be noted that even on a flat obstacle the jet flow structure is rather complex, and it has several characteristic regions, whose main scale (as the investigations of different authors have shown) is the jet diameter. If the obstacle is a spherical cavity, then new scales appear — the depression diameter and depth — and their manifestation in the flow structure is of undoubted interest.

The program of the present investigations is a sequel of our work [12]. It included two sets of experiments. In the first set we studied the interaction of an impinging jet with a flat surface and in the second one — with spherical cavities with a different depth. This enabled us to compare the measurement data and reveal the influence of the surface curvature on the flow and heat exchange. We carried out black-oil visualization of the wall streamlines and measured the radial distributions of pressures near the cavity surface and the local heat transfer both in the cavity and outside it. In so doing, we used, as variable parameters, the Reynolds number of the jet and the distance from the nozzle exit section to the obstacle.

Description of the Experimental Facility and Measuring Techniques. The experiments were performed on the facility schematically represented in Fig. 1. An axisymmetric air jet of room temperature flows out of a nozzle of diameter d_n = 8.5 mm.The gas velocity in the nozzle exit section U_n varies between 28 and 100 m/sec, and the corresponding value of the Reynolds number $\mathrm{Re} = U_n d_n/\nu = 10^4$–$6\cdot10^4$. The degree of reduction of the flow in the nozzle is ≈8, and the nozzle is smoothly contoured; therefore, the velocity distribution in its exit section is practically uniform, and the turbulence intensity Tu ≅ 0.3%. The jet impinges on the obstacle at a right angle, and the distance from the nozzle to the obstacle S is varied from 0 to $10d_n$.

The first stage of the work was devoted to hydrodynamic investigations and included black-oil visualization of the pattern of streamlines near the obstacle surface and the investigation of the static pressure distributions on the obstacle. In these experiments, the obstacle was an organic-glass disk of diameter 70 mm with a spherical cavity of diameter 46 mm and depth 6 and 23 mm (ΔD_c = 0.12 and 0.5) cut in the center. As tests, experiments on a flat surface

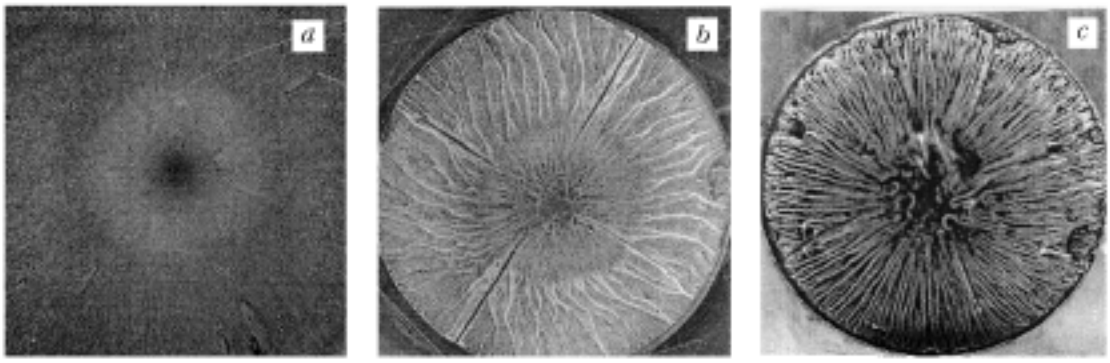

Fig. 2. Results of the visualization investigations (Re = $2.8 \cdot 10^6$; $S/d_n = 2$): a) flat obstacle; b, c) depression ($\Delta/D_c = 0.12$ and 0.5, respectively).

were carried out. Along the radial direction on the obstacle, normally to its curvilinear surface, three holes of diameter 0.5 mm were drilled for pressure relief.

To visualize the flow, smooth adhesive film was pasted onto the surface of obstacles and a mixture of burning kerosene with black offset ink was applied to it. In the course of the experiment, which lasted 1–1.5 min, the working mixture poured on the obstacle uniformly covered its entire surface and the pattern of the streamlines stabilized.

The second set of experiments was devoted to the heat exchange on the obstacle. In these experiments, the working part of diameter 190 mm and thickness 50 mm was made of copper. The required temperature difference between the jet and the obstacle, which in the majority of cases was equal to 40^o, was attained by means of an electric heater located under the obstacle. The choice of high-heat-conductivity copper as a material fulfilled the boundary condition on the obstacle $T_w \cong$ const. The temperatures of the flown wall and the flow was controlled by chromel-copel thermocouples. Measurements of the local heat flows were made with the help of gradient thermal flow sensors glued to the obstacle [13]. The sensors had the following characteristics: dimensions in plan of no more than 2.5 × 2.5 mm (which is much less than the characteristic size of the investigated flow), thickness of ≈0.2 mm, volt-ampere sensitivity of ≈10 mV/W, time constant of the order of 0.05 msec. They were intended for obtaining arrays of instantaneous values of the heat flow densities and determining, on their basis, the time-average heat flows, as well as their pulsations and spectra. The number of realizations within one measurement was chosen to be equal to 10^4, and the time of one measurement was varied from 10 to 90 sec and, as the experiments show, it influenced the results of measurements only slightly. Through an ad hoc multichannel module signals from the thermocouples and sensors were amplified, arrived at the computer, and were processed there. Analysis has shown that the measurement error for the heat flow densities was in the 0.3–10% range and for the intensity of rms fluctuations of the heat flow density it turned out to differ widely for measurements on a flat obstacle and on an obstacle with a depression: in the first case it could reach 100%, and in the second case is varied from 4 to 30%.

Experimental Results and Discussion. *Visualization of the flow.* The typical pattern of the flow past obstacles of different configurations when they were located in the initial segment of the jet is given in Fig. 2. It is seen that on the flat obstacle (Fig. 2a) the flow is broken up into three characteristic regions: the central region ($r/d_n \le 0.3$) where the jet impinges on the wall and makes a turn to form Taylor–Goertler vortices; the circular region ($0.3 \le r/d_n \le 1.2$) where, according to [14], a laminar (accelerated) boundary layer develops and decays; and the remainder of the surface ($r/d_n > 1.2$) where the flow conditions become turbulent. The same pattern on a flat obstacle can also be seen in monograph [14].

The flow pattern in depressions, being similar in appearance to the above pattern, is, nevertheless, different (see Fig. 2b and c). The most pronounced differences are observed in a hemispherical depression: 1) the central region, where Taylor–Goertler vortices are formed and decay, has markedly widened (from $0.35d_c$ to $0.7d_c$); 2) at the exit from the depression (r/d_n = 2.6–2.7) a stagnation region has appeared (dark narrow ring in the photograph); 3) between the central and stagnation regions of the flow there is now a region characterized by pronounced oscillations of the flow.

It is known [15] that the distribution of the heat transfer coefficient over the surface of a flat obstacle is nonuniform and under certain conditions two peaks are observed in it: the first peak (at $r/d_n \cong 0.5$) is associated with

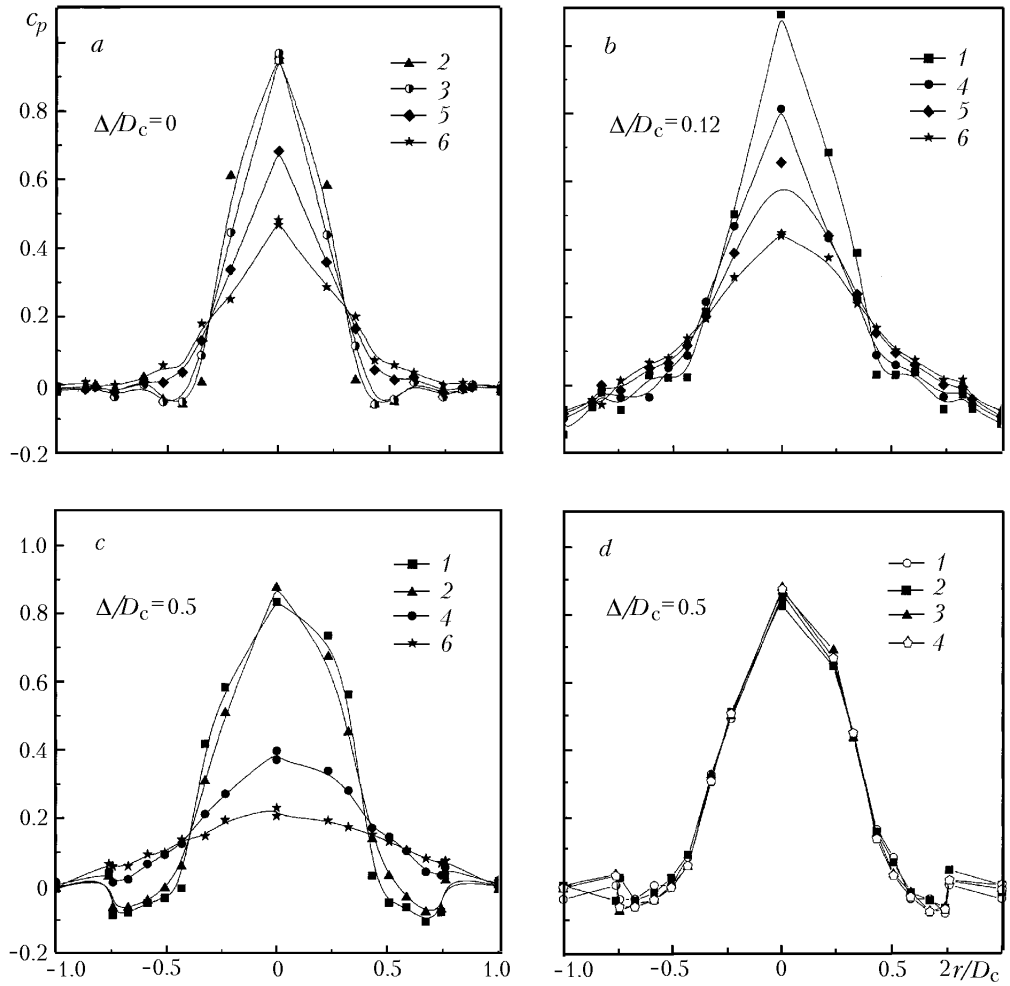

Fig. 3. Radial distribution of the pressure coefficient on the obstacle: a, b, c) Re = $2.9 \cdot 10^4$ [1) S/d_n = 0; 2) 2; 3) 4; 4) 6; 5) 8; 6) 10]; d) S/d_n = 2 [1) Re = $1.2 \cdot 10^4$; 2) $1.6 \cdot 10^4$; 3) $2.3 \cdot 10^4$; 4) $2.9 \cdot 10^4$].

the pressure gradient maximum, and the second one (more distant from the center) — with the switch of the flow from laminar conditions to turbulent ones (see, e.g., [15, 16]). The visualization results in these experiments suggest that one possible reason for the appearance of the first peak of heat transfer is the formation and decay of Taylor–Goertler vortices. Evidently, the same nonstationary process caused the variations in pressure observed by us.

If the obstacle was located beyond the initial segment of the jet measuring, according to [15], 5–6 diameters of the nozzle, then, as a result of turbulence of the whole flow region, the pattern of the spread of the black-oil mixture on obstacles was indeterminate and no clearly defined zones were observed.

Pressure distribution over the surface. The pressure fields were investigated with varied distance from the nozzle to the obstacle (S/d_n = 0–10) and Reynolds number (Re = $(1–3) \cdot 10^4$). The experiments corresponding to the distance S/d_n = 0 were performed only for the flow past cavities, and in this case the nozzle was positioned flush with the flat part of the obstacle surface. The pressure coefficient was determined by the pressure difference on the surface P_i and in the environment P_a referred to the impact gas pressure in the nozzle exit section:

$$C_{pi} = 2\,(P_i - P_a)/(\rho_n U_n^2)\,.$$

The radial distributions of the pressure coefficient are given in Fig. 3. It is seen that for all investigated obstacles and flow conditions in the immediate vicinity of the frontal point C_p the distributions have a qualitatively similarly dome-shaped form with a vertex on the jet axis, where the quantity C_p in the region of the initial segment of the

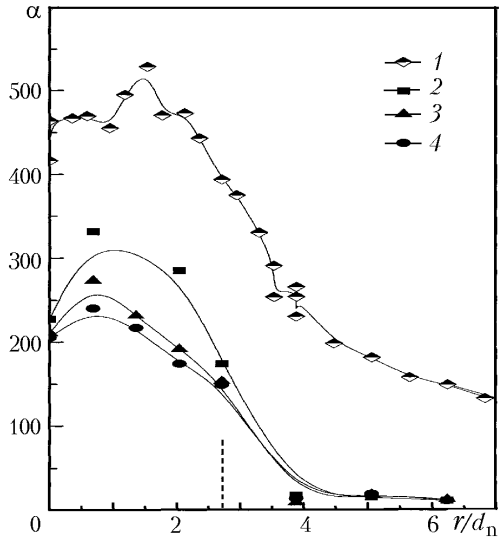

Fig. 4. Radial distribution of the heat transfer coefficient, Re = $2.8 \cdot 10^4$: 1) flat obstacle, S/d_n = 2; 2–4) depression-containing obstacles ΔD_c = 0.5 [2) S/d_n = 0; 3) 2; 4) 6. Dashed line marks the depression boundary.

jet is close to unity. At the same time, at the obstacle periphery ($0.5 \le 2r/D_c \le 1$) the character of the distributions of pressure coefficients depends on the depression depth and the nozzle-to-obstacle distance. For instance, in a depression of depth Δ/D_c = 0.12 (Fig. 3b) the region of accelerated flow extends up to the cavity boundary ($2r/D_c$ = 1), and on a flat surface (Fig. 3a) it is bounded by the value of $2r/D_c \le 0.5$. The local minima of C_p formed at the obstacle periphery on a curvilinear surface are not as clearly defined as on a flat one.

In a hemispherical depression (Δ/D_c = 0.5, Fig. 3c), the pressure coefficient distributions in the vicinity of the frontal point are also dome-shaped, but they are filled to a greater extent compared to a flat surface, and the radial pressure gradients markedly increase. About a quarter of the radius is occupied by the rarefaction region, and then the pressure regains the atmospheric value, leading to a flow separation. Such interpretation of the results is confirmed by the visualization pattern in Fig. 2c, where the cavity periphery is not painted and, consequently, the gas flow does not penetrate into this region.

It should be noted that the radial distributions of the pressure coefficient corresponding to different values of the Reynolds number coincide with one another, which points to a self-similar flow with respect to this parameter. This is clearly evidenced by the data given in Fig. 3d.

As mentioned above, under certain conditions impinging jets and depressions can generate specific oscillation regimes and coherent structures. Likewise, in our experiments pressure oscillations were registered, and they were observed both on a flat obstacle and in depressions. These oscillations were rather low-frequency (≈1 Hz) and arose at certain values of the parameters Re and S/d_n (different on the flat obstacle and in the depression) in a small vicinity around the frontal point ≈(1–2)d_n. The oscillation intensity was low (fractions of a percent of the measured pressure), but in the depression it was 1.5–3 times higher than on the flat wall.

Heat exchange. The main heat transfer measurements were taken for two "limiting" cases: on a flat obstacle (Δ/D_c = 0) and on an obstacle with the deepest — hemispherical — depression (Δ/D_c = 0.5). The local values of the heat transfer coefficients were determined by the measured heat flow density q_i decreased by the value of the heat flow density due to the free convection and radiative heat exchange Δq_i and the temperature difference between the surface and the air in the jet mouth:

$$\alpha_i = (q_i - \Delta q_i)/(T_w - T_n) .$$

The correction value of Δq_i was determined experimentally by measuring the heat exchange on the model in the absence of a jet flow and constituted 5–7% of the value of the heat flow density at the frontal point.

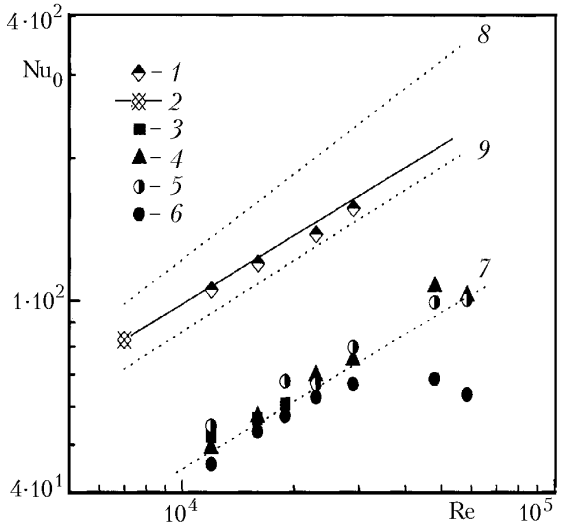

Fig. 5. Heat transfer at the frontal point of the flat obstacle and depression: 1, 2) flat obstacles, S/d_n = 6 [1) our experiment; 2) experiment of [18]]; 3–6) obstacles with a depression; Δ/D_c = 0.5 [3) S/d_n = 0; 4) 2; 5) 4; 6) 6]; 7) generalization of the experiments in the depression; 8) dependence (2); 9) dependence (3).

The distribution of the local values of the heat transfer coefficient along the flat surface radius and the hemispherical depression radius is given in Fig. 4. It is seen that the heat exchange intensity in the investigated cavity is practically twice lower than on the flat surface. This is explained by the difficulty of penetration of the jet flow into the depression and, as a result, by the decrease in the intensity of the processes of heat transfer between the jet and the surface. However, if we take into account that the hemispherical cavity surface is twice larger than the flat surface, then the integral value of the heat transfer from the depression remains the same as on the flat surface.

As would be expected, with increasing nozzle-obstacle distance (with increasing parameter S/d_n) the heat transfer in the cavity becomes less intensive. At the same time, outside the depression at all distances heat transfer is practically absent. The probable reason for the extremely low heat transfer outside the cavity is the formation of a stagnation region here. The air stream entering the cavity in the vicinity of the frontal point flows out of it along the generating line, i.e., with respect to the cavity geometry, counter to the falling jet flow. As a result of this, the process of jet spreading outside the cavity is practically not observed. The thus formed flow had an effect on the distribution of the heat transfer coefficients. Evidently, the strong suppression of the heat transfer revealed in the experiments can be used effectively in high-temperature devices, where the problem of reducing heat flows into the wall exists, e.g., in plasmatrons [17].

The generalized data on the heat transfer at the stagnation point for the flat and hemispherical surfaces are given in Fig. 5. The experimental results for the flat surface are in good agreement with the classical results of [18] and are described by the empirical formula

$$\mathrm{Nu}_0 = 1.24\mathrm{Pr}^{0.33}\mathrm{Re}^{0.5}\,(S/d_n)^{-0.11}\,. \qquad (1)$$

For the hemispherical cavity, the experimental points are situated much lower, but the slope of the correlation dependence $\mathrm{Nu}_0 \approx \mathrm{Re}^n$ (the generalizing line (7)) remains the same (n = 0.5), which points to a similarity of the heat transfer mechanisms at the critical point on the surface and in the depression.

For comparison, Fig. 5 presents the results of the experimental investigations of the heat transfer at the stagnation point of a jet impinging on a hemispherical cavity in [11]. The distinguishing feature of this work is the large diameter ratio between the cavity and the nozzle (D_c/d_n = 16–44). In our experiments, the ratio D_c/d_n was much smaller and equalled 5.4. The results of [11] are given in Fig. 5 by lines 8 and 9 for S/d_n = 6 and two extreme values of D_c/d_n equal to 44 and 16, respectively. At the smallest diameter of the nozzle (D_c/d_n = 44) the heat transfer

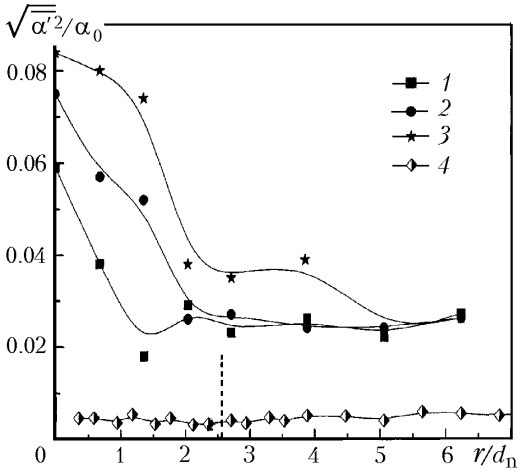

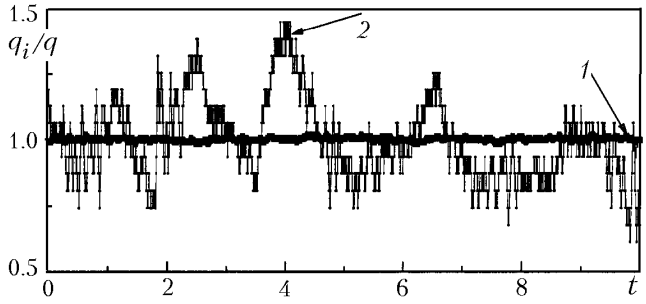

Fig. 6. Radial distribution of pulsations of the heat transfer coefficient on an obstacle with a depression and a flat obstacle: 1–3) obstacles with a depression, Δ/D_c = 0.5 [1) S/d_n = 0; 2) 6; 3) 10]; 4) flat obstacle, S/d_n = 2; Re = $2.8 \cdot 10^4$.

Fig. 7. Time scan of the signal from the heat flow sensors located at a distance of $1/4d_n$ from the frontal point, Re = $2.8 \cdot 10^4$; S/d_n = 2; 1) flat obstacle; 2) depression. Δ/D_c = 0.5.

intensity at the frontal point of the hemispherical depression exceeds the value on the flat surface, and the Reynolds number exponent also changes therewith:

$$\mathrm{Nu}_0 = 0.798\mathrm{Re}^{0.604}\mathrm{Pr}^{0.4}\,(S/d_n)^{-0.22}\,. \tag{2}$$

As the nozzle diameter increases (line 9), the heat transfer weakens and the experimental data take an intermediate position between the values for the small nozzle and the results of the present work, where the diameter ratio between the cavity and the nozzle was the smallest (D_c/d_n = 5.4). In [11], the experimental data for relatively large nozzles (and $3 < S/d_n < 7$) are described by the empirical relation

$$\mathrm{Nu}_0 = 0.666\mathrm{Re}^{0.5}\mathrm{Pr}^{0.4}\,(S/d_n)^{0.17}\,(d_n/d_{jet})^{0.07}\,. \tag{3}$$

In calculating line 9 with allowance for the condition S/d_n = 6, $d_{jet} \approx 2d_n$ was assumed. As is seen, with increasing nozzle diameter the Reynolds number exponent becomes equal to n = 0.5 (the same as on the flat surface), and the dependence on the nozzle-cavity distance reverses.

The above features of the distributions of the heat transfer coefficients point to an extremely complex and multifactor mechanism of heat transfer under a jet flow past spherical depressions. Indeed, besides the parameters that have manifested themselves under interaction of impinging jests with flat surfaces, a strong influence on the heat transfer in the depression is produced by the ratio D_c/d_n, as well as by Δ/D_c (or Δ/d_n).

On the basis of the processed arrays of instantaneous values of the heat flow density measured by the sensors we estimated the local rms pulsations of the heat flow density and the heat transfer coefficient. Figure 6 shows the radial distributions of pulsations of the heat transfer coefficient on flat and depression-containing surfaces.

To normalize pulsations, the value of the transfer coefficient at the frontal point α_0 was used. Throughout the flat obstacle surface pulsations of the heat transfer coefficients change only slightly and are within 1% of the value of α_0. The pulsation intensity of the heat transfer coefficient on the surface with a depression is everywhere higher than on the flat wall; it changes only slightly outside the depression, and increases when moving from the cavity periphery to the frontal point. The large values of pulsations inside the depression are caused by the formation in it of nonsta-

tionary coherent structures. The character of pulsation distributions on the spherical cavity surface remained constant with changing Reynolds number.

The formation of coherent structures in the depression is confirmed by the analysis of the time scans of signals from the heat flow sensors constructed for various positions on the obstacle and under different flow conditions. A typical time scan of the heat flow sensor signal is shown in Fig. 7. It can be seen that the sensor signal looks as if it has been modulated by large-scale low-frequency oscillations. The spectral analysis of the data of Fig. 7 has made it possible to estimate the modulation frequency (of the order of 1 Hz).

CONCLUSIONS

1. On a flat obstacle located in the initial segment of the jet, the visualization investigations have revealed three regions: the central region ($r/d_n \le 0.3$) filled with Taylor–Goertler vortices; the circular region ($0.3 < r/d_n \le 1.2$) where the laminar-flow conditions become turbulent, and the region of zero-gradient pressure ($r/d_n > 1.2$). For the same conditions in a spherical cavity the central region widens, at the exit from the depression a circular stagnation region arises, and between the central and stagnation regions now there lies a region characterized by pronounced flow oscillations.

2. In the region of $r/d_n \le D_c/2$, the local values of the heat transfer coefficient in the hemispherical cavity flown by a jet are about twice lower than under identical conditions on the flat obstacle; however, the total heat transfer from it with allowance for the enlargement of the surface area at the cost of the depression is the same as on the flat obstacle.

3. The intensity of rms pulsations of the heat flow density on the flat obstacle is low. The pulsations on the cavity-containing obstacle are mush higher, which is due to the formation in the depression cavity of nonstationary coherent structures.

This work was supported by a grant to leading scientific schools of the Russian Federation (project NSh-1308.2003.8) and grants of the Russian Foundation for Basic Research (project No. 04-02-16070 and No. 04-02-08250 ofi-a).

NOTATION

C_p, pressure coefficient; d_n, d_{jet}, and D_c, diameters of the nozzle, the jet near the obstacle, and the spherical cavity, mm; n, exponent; $Nu = \alpha d_n/\lambda$, Nusselt number; Pr, Prandtl number; P, pressure, Pa; q, density of the heat flow through the wall, W/m^2; r, radial distance from the frontal point, mm; $Re_D = U_n D_c/\nu$, $Re = U_n d_n/\nu$, Reynolds numbers; S, nozzle-to-obstacle distance, mm; t, time, sec; T, temperature, ^oC; Tu, degree of turbulence; U, velocity, m/sec; α, heat transfer coefficient, W/(m$^2\cdot^o$C); Δ, depression depth, mm; Δq, heat flow density due to free convection and radiation, W/m^2; λ, heat conductivity coefficient, W/(m$\cdot^o$C); ν, kinematic viscosity of flowing air, m^2/sec; ρ, air density, kg/m^3. Subscripts: a, atmosphere; c, cavity; p, pressure; n, nozzle; jet, jet near the obstacle; w, wall; i = 0, 1, 2, ..., various positions on the obstacle beginning from the frontal point.

REFERENCES

1. Terekhov and S. V. Kalinina, Flow structure and heat transfer under a flow past an individual spherical cavity. State-of-the-art and problems (Review), *Teplofiz. Aéromekh.*, **9**, No. 4, 497–520 (2002).
2. V. N. Afanasyev, Y. P. Chudnovsky, A. I. Leontiev, and P. S. Roganov, Turbulent flow friction and heat transfer characteristics for spherical cavities on a flat plate, *Exp. Thermal Fluid Sci.*, **7**, 1–8 (1993).
3. G. I. Mahmood and P. M. Ligrani, Heat transfer in a dimpled channel: Combined influences of aspect ratio, temperature ratio, Reynolds number, and flow structure, *Int. J. Heat Mass Transfer*, **45**, No. 10, 2011–2020 (2002).
4. Ch.-M. Ho and N. S. Nosseir, Large coherent structures in an impinging jet, in: *Proc. Second Int. Symp. on Turbulent Shear Flows "Turbulent Shear Flows 2,"* London, July 1979, Berlin, 1980, pp. 297–304.

5. S. Alekseenko, A. Bilsky, O. Heinz, B. Ilyushin, and D. Markovich, Near-wall characteristics of impinging turbulent jet, in: *Proc. Fourth Int. Symp. on Turbulence, Heat and Mass Transfer*, 12–17 October 2003, Antalya, Turkey, pp. 235–241.
6. L. Tianshu and J. P. Sullivan, Heat transfer and flow structures in an excited circular impinging jet, *Int. J. Heat Mass Transfer*, **39**, No. 17, 3695–3706 (1996).
7. D. Kokh and D. Hartnet, Measurement of pressure distribution and local heat transfer under a flow past concave hemispheres, *Raketn. Tekhn. Kosmonavt.*, **31**, No. 1, 86–91 (1961).
8. E. M. Sparrow and G. T. Geiger, Heat transfer at the base of a cylindrical cavity oriented perpendicular to a freestream flow, *Int. J. Heat Mass Transfer*, **28**, No. 12, 2353–2361 (1985).
9. Y. Kornblum and R. J. Goldstein, Jet impingement on semicircular concave and convex surface, Part one: Recovery factor, in: *Proc. Int. Symp. on the Physics of Heat Transfer in Boiling and Condensation*, Moscow, 1997, pp. 597–602.
10. Y. Kornblum and R. J. Goldstein, Jet impingement on semicircular concave and convex surface, Part two: Heat transfer, in: *Proc. Int. Symp. on the Physics of Heat Transfer in Boiling and Condensation*, Moscow, 1997, pp. 603–608.
11. P. Hrycak, Heat transfer and flow characteristics of jets impinging on a concave hemispherical plate, in: *Proc. 7th Int. Heat Transfer Conf.,* Munchen, Hemisphere Publ. Corp., Washington–New York–London, 1982, Vol. 3, pp. 357–362.
12. V. I. Terekhov, V. L. Barsanov, S. V. Kalinina, and Yu. M. Mshvidobadze, Study of flow structure and heat transfer under normal jet flow of a spherical cavity, in: *Proc. XXVII Siberian Seminar on Thermal Physics* [in Russian], IT SO RAN, Novosibirsk (2004), CD-ROM, No. 143.
13. S. Z. Sapozhnikov, V. Yu. Mityakov, and A. V. Mityakov, *Gradient Flow-Sensing Elements* [in Russian], St. Petersburg (2003).
14. B. N. Yudaev, M. S. Mikhailov, and V. K. Savin, *Heat Transfer under Interaction between Jets and Obstacles* [in Russian], Mashinostroenie, Moscow (1977).
15. E. P. Dyban and A. I. Mazur, *Convective Heat Transfer under a Jet Flow past Bodies* [in Russian], Naukova Dumka, Kiev (1982).
16. J. Lee and S.-J. Lee, The effect of a nozzle configuration on stagnation region heat transfer enhancement of axisymmetric jet impingement, *Int. J. Heat Mass Transfer*, **43**, 3497–3509 (2000).
17. M. F. Zhukov (Ed.), *Plasmatrons. Studies. Problems* [in Russian], Novosibirsk (1995).
18. R. Gardon and J. Cobonque, Heat transfer between a flat plate and jets of air impinging on it, in: *Proc. Int. Heat Transfer Conf. "International Development in Heat Transfer,"* New York (1961), pp. 454–460.